



TECHNICAL ARTICLE

Additive Manufacturing of Compliant Mechanisms for Deployable Aerospace Structures

Christine A. Gebara, Paul D. Lytal, and Julian J. Rimoli

Submitted: 15 September 2021 / Revised: 16 May 2022 / Accepted: 21 May 2022 / Published online: 27 June 2022

In the past 10 years, complex deployable structures have become common on CubeSats and large-scale spacecraft. As new missions are pursued, there is an increased need for more mass and volume efficient deployments. Over the same period, metal additive manufacturing (AM) has enabled new forms of spaceflight hardware. However, AM of compliant mechanisms has not been fully leveraged for deployable aerospace structures. The Surface Water Ocean Topography and NASA-ISRO Synthetic Aperture Radar mission missions launching in 2022 both utilize large deployable masts. Each mast deployment is driven by numerous spring and damper mechanisms. Because of volume constraints, the spring mechanisms designed utilize high aspect ratio rectangular cross section torsion springs that represent the state of the art of manufacturing. This extreme spring design resulted in manufacturing difficulties and hardware failures during ground mechanism testing. Upon re-examining the mechanism design, AM enables torque performance, mass, and complexity improvements. AM allows for torsion spring cross sections not otherwise possible with traditional spring manufacturing methods. Prototype springs of various cross sections were printed in maraging steel and tested. Results confirmed design analysis, and doubling of the spring constant was achieved when compared to the traditional springs. The use of AM also allows springs to be built monolithically with surrounding structure. Design, manufacturing, and test findings will be discussed along with future implications for deployable aerospace structures.

Keywords aerospace, additive manufacturing, mechanical systems, mechanical testing, steel

1. Introduction

With the development of additive manufacturing (AM), fabrication constraints have relaxed. It is now possible to manufacture new types of geometries, materials, and components not otherwise possible with subtractive manufacturing. This progress enables a new class of space systems to be imagined. Furthermore, the infusion of AM into industry has corresponded with deployable aerospace structures becoming increasingly common on spacecraft of all sizes. AM can be

This invited article is part of a special issue in the *Journal of Materials Engineering and Performance* entitled “Space and Aerospace Exploration Revolution: Metal Additive Manufacturing.” The issue was organized by Shahrooz Nafisi, Relativity Space; Paul Gradl, NASA Marshall Space Flight Center; Douglas Hofmann, NASA Jet Propulsion Laboratory/California Institute of Technology; and Reza Ghomashchi, The University of Adelaide, Australia.

The research was carried out at the Jet Propulsion Laboratory, California Institute of Technology, under a contract with the National Aeronautics and Space Administration (80NM0018D0004).

Christine A. Gebara and **Paul D. Lytal**, Jet Propulsion Laboratory, California Institute of Technology, Pasadena, United States; and **Julian J. Rimoli**, Guggenheim School of Aerospace Engineering, Georgia Institute of Technology, Atlanta, United States. Contact e-mail: Christine.a.gebara@jpl.nasa.gov.

leveraged to minimize part count, mass, and volume of deployable structures. (Ref 1, 2, 3) To achieve the ultimate goal of being able to additively manufacture entire spacecraft systems, development of AM compliant elements must be to mature the technology. This report will take an existing deployable structure mechanism and modify the design to leverage additive manufacturing.

2. Traditional Mechanism

NASA’s Jet Propulsion Laboratory is developing two earth orbiting satellites. The Surface Water Ocean Topography (SWOT) mission will conduct the first global survey of Earth’s surface water. (Ref 4) The NASA-ISRO Synthetic Aperture Radar (NISAR) mission will study temporal changes to Earth’s land and ice-sheets using advanced radar techniques. (Ref 5) Both SWOT and NISAR use deployable radar reflector masts with differing geometries, but similar components and sub-assemblies. Operationally, the masts are launched in a stowed state with a launch restraint system. When commanded, the restraints release a pre-tensioned spring and damper mechanism which deploys each hinge.

3. Traditional Mechanism Design and Fabrication

Each hinge for the SWOT and NISAR masts is outfitted with a spring, damper, and potentiometer mounted coaxially with each hinge line. The NISAR mast is composed of 0.178 m square composite tubing. The SWOT mast is composed of

0.254 m square composite tubing. Figure 1 displays the spring mechanisms for each mission. Ultimately, this led to a cylindrical volume allowance of 0.178 m in length and 0.045 m in diameter for the NISAR spring mechanism. The NISAR mechanisms can be seen in Fig. 2.

Per JPL design requirements for mission critical mechanisms, the springs are required to have a minimum “no test” yield factor of safety (FS) of 1.50 and an ultimate FS of 1.65. Furthermore, JPL design principles impose a minimum mechanism torque margin of 100% in worst case environments. These requirements ultimately meant the mechanism needed to produce a minimum deployment torque of 3.16 N*m at hinge closure. To meet these requirements, a 17-7 steel spring was designed with a rectangular cross section aspect ratio of 3.88:1. This aspect ratio was determined to be the state of the art for spring winding manufacturing.

The rectangular spring cross section caused numerous issues for mechanism development despite a successful prototype test campaign. The initially manufactured springs exceeded axial length requirements. Furthermore, the spring wire was prone to unexpected twisting during winding. Once the flight mechanisms were assembled, a hardware failure was observed during thermal performance testing. From repeated spring cycling, fragmented Teflon Foreign Object Debris (FOD) was generated. This can be seen in Fig. 3. The FOD was determined to come from glass-filled Teflon sleeve bearings sitting below each spring. Ultimately, the Teflon sleeve bearing with a grease-plated 440C stainless steel sleeve bearing with modified geometry. (Ref 6, 7)

4. Spring Theory

To alleviate the issues encountered with the traditionally fabricated spring mechanism, the application of additive manufacturing will be studied to improve torque performance, mass, and volume. Torsion springs are normally cold wound or machined. As such, spring design has generally been limited to round or rectangular cross sections. This is because most applications allow for an increase in stock wire size if performance is not adequate. As previously stated, for the SWOT and NISAR missions, the design was volume constrained and torque dependent.

4.1 Spring Design Methodology

A torsion spring can be modeled as a beam under constant moment. Therefore, the maximum stress, σ , can be modeled using eq 1. Variable M represents the maximum applied moment. Variable I represents the cross-sectional moment of inertia. Variable c represents the distance from the cross-sectional neutral axis. Variable K represents the Wahl stress concentration factor defined in eq 2. This is an analytically derived factor that accounts for increased stress in eq 1 due to the effect of direct shear and change in spring coil curvature. This factor is calculated using the spring index, C , defined as the ratio of spring coil diameter to wire diameter.

$$\sigma = K \frac{Mc}{I} \quad (\text{Eq 1})$$

$$K = \frac{(3C^2 - C - 0.8)}{(3C(C - 1))}. \quad (\text{Eq 2})$$

Using beam theory, the deflection of the spring, θ_e , can be calculated using eq 3. Here, moment is replaced with the equivalent force, F , multiplied by length of the spring wire, l . The material elastic modulus is represented by E .

$$\theta_e = \frac{y}{l} = \frac{Fl^2}{3EI}. \quad (\text{Eq 3})$$

Spring end conditions must also be accounted for. The deflection of the cantilevered beams (for straight torsion spring arms) can be accounted for using eq 4. Where l_1 and l_2 represent the length of each spring end. θ_1 and θ_2 represent the deflection of each end, respectively.

$$\theta_1 = \frac{Ml_1^2}{3EI} \quad \theta_2 = \frac{Ml_2^2}{3EI}. \quad (\text{Eq 4})$$

Ultimately, the total deflection, θ_T , of the spring can be calculated by summing all deflections.

$$\theta_T = \theta_1 + \theta_2 + \theta_e. \quad (\text{Eq 5})$$

The spring rate, k , can now be calculated using eq 6.

$$k = \frac{M}{\theta_T}. \quad (\text{Eq 6})$$

With this formulation, springs can be designed without being limited to round and rectangular cross sections, taking advantage of AM design flexibility. (Ref 8, 9)

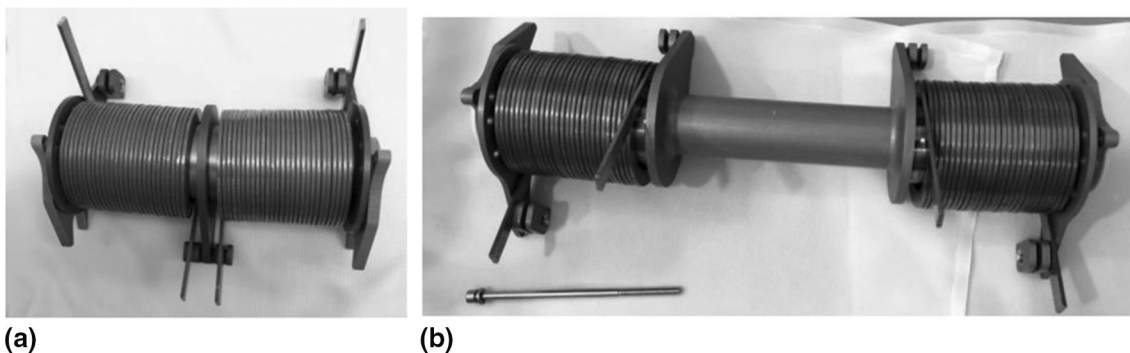


Fig. 1 View of (a) NISAR (0.116 m in length) and (b) SWOT (0.192 m in length) spring mechanisms demonstrating differences in overall length and relaxed spring arm position

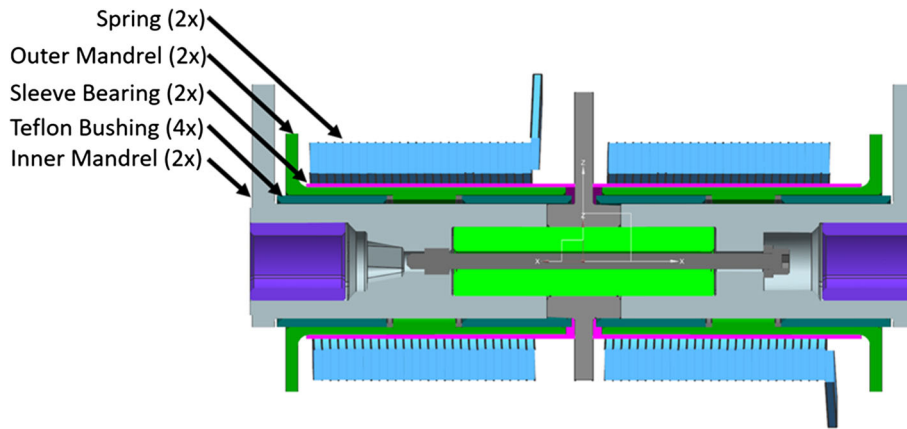


Fig.2 Cross section of NISAR spring mechanism



Fig. 3 Image of spring mechanism during thermal testing with hardware failure circled

Table 1 Traditional flight hardware material compared to AM EOS MS1 (Ref 10)

	Units	17-7 CH900	EOS MS1
Elastic modulus	GPa	204.0	180.0
Yield strength	MPa	1930	1986
Ultimate strength	MPa	2010	2048

5. Design for Additive Manufacturing

To leverage the full potential of AM, designs must simultaneously consider mechanism design, process design, and material consideration.

5.1 Material and Process Selection

For the sake of this study, direct energy deposition (DED) and laser bed powder fusion (LBPF) processes and materials were considered. DED and LBPF are the most developed AM processes for aerospace applications as far as material development, processes maturity, quality control, and manufacturing availability. Further, material properties were taken from available literature. Ultimately, EOS MS1 maraging steel was selected because of its high performance. Table 1 compares traditional spring material to EOS MS 1.

A consideration for material and process selection is fatigue life. The original spring had a much higher fatigue life (> 10,000 cycles) than needed for the flight application. The mechanism is only deployed once in space and tested up to 20

times on the ground. Generally, AM is assumed to result in lower fatigue life compared to traditional materials because of the assumed higher surface roughness and the increased possibility of subsurface defects. (Ref 11) For an AM torsion spring, the engineering trade to exchange fatigue life for design flexibility must be evaluated.

5.2 Spring Design

Leveraging AM, many types of spring cross sections are now possible to fabricate. In this application, torque performance and volume are the driving design factors. To maximize cross-sectional moment of inertia, an *I*-beam section may be leveraged. However, this design becomes less attractive when considering friction between spring windings. Remaining with a rectangular cross section, AM enables a higher cross-sectional aspect ratio than otherwise possible with the current state of the art of cold wound springs. By increasing the height of the rectangular section from 5.3 to 7.0 mm while minimizing the section width from 1.4 to 1.2 mm, stress decreases notably if torque output is held constant. Further, the ability to round corners of the cross section alleviates the issues experienced with the traditional mechanism.

Using Advanced Spring Design 7 software, several springs were designed and analyzed in preparation for manufacturing. These springs are shown in Table 2 compared to the “baseline” spring that will fly on the SWOT and NISAR missions. The springs analyzed were incrementally changed with respect to each other. Because of budgetary constraints, not all springs were manufactured. This will be discussed in following sections. For all designs, 27.25 spring body windings were used. For round wire torsion springs, “line” contact is formed

between the windings. For rectangular contact springs, “surface” contact is formed between the windings, increasing friction. However, with AM, rectangular cross sections can be modified to minimize contact between windings. “Standoff” features can also be added to remove surface rubbing and form line contact between windings. This can be seen in the final design of Table 3.

6. Manufacturing and Testing

6.1 Manufacturing and Inspection

The springs were fabricated on EOS LBPf printers at two vendors. The vendors each selected printing parameters and heat treat to EOS MS1. Figure 4 shows the visual difference as a result of different heat treat methods. Vendor #1 had previous

experience using maraging steel powder, and had developed custom parameters for their EOS M290 printers. The springs were fabricated using powder from Carpenter Additive with a

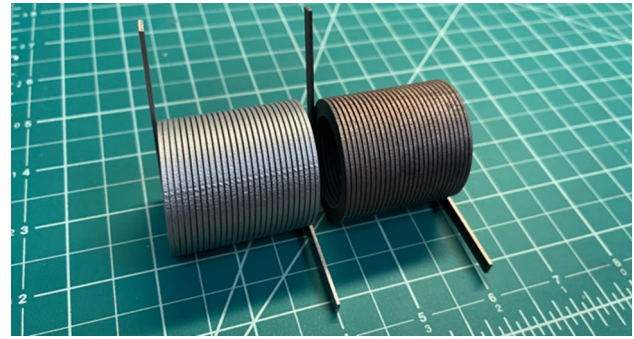


Fig. 4 Vendor #1 spring (left) and Vendor #2 spring (right)

Table 2 Summary of design variables for springs tested

		1.4 mm	1.4 mm	1.4 mm	1.4 mm	1.2 mm
		5.3 mm	5.3 mm	7.0 mm	9.0 mm	7.0 mm
		Baseline	1:1 Swap	Increase radial height step 1	Increased radial height step 2	Minimized thickness, increased height
Material		17-7 PH CH900	EOS MS1	EOS MS1	EOS MS1	EOS MS1
Spring constant	N*m/rad	1.0	0.9	2.0	4.1	1.7
Displacement at 2.26 N*m	Rad	2.1	2.4	1.1	0.6	1.3
Max torque out (180 deg past minimum torque needed)	N*m	5.5	5.2	8.6	15.0	7.7
Yield stress margin (1.5 FOS)	%	53%	69%	76%	66%	69%
Ultimate stress margin (1.65 FOS)	%	45%	58%	65%	56%	58%

Table 3 Spring torque performance test results

		Baseline	1:1 Swap (vendor A)	:1 Swap (vendor A)	Increase radial height	Thickness change, increased height, friction feature
Manufacturer		Traditional vendor	AM vendor 1	AM vendor 2	AM vendor 1	AM vendor 1
Quantity tested		6	4	4	4	4
Material		17-7 PH CH900	EOS MS1	EOS MS1	EOS MS1	EOS MS1
Cross section width, axial	mm	1.40	1.40	1.40	1.40	1.20
Cross section height, radial	mm	5.33	5.33	5.33	7.00	7.00
Design spring constant	N*m/rad	0.971	0.932	0.932	2.020	1.729
Experimental spring constant	N*m/rad	1.146	1.120	1.139	2.480	2.136
% experimental spring constant compared from design	%	+18%	+20%	+22%	+22%	+24%
% spring constant experimental compared to baseline	%	0.00%	-2.2%	-0.56%	+76%	+50%

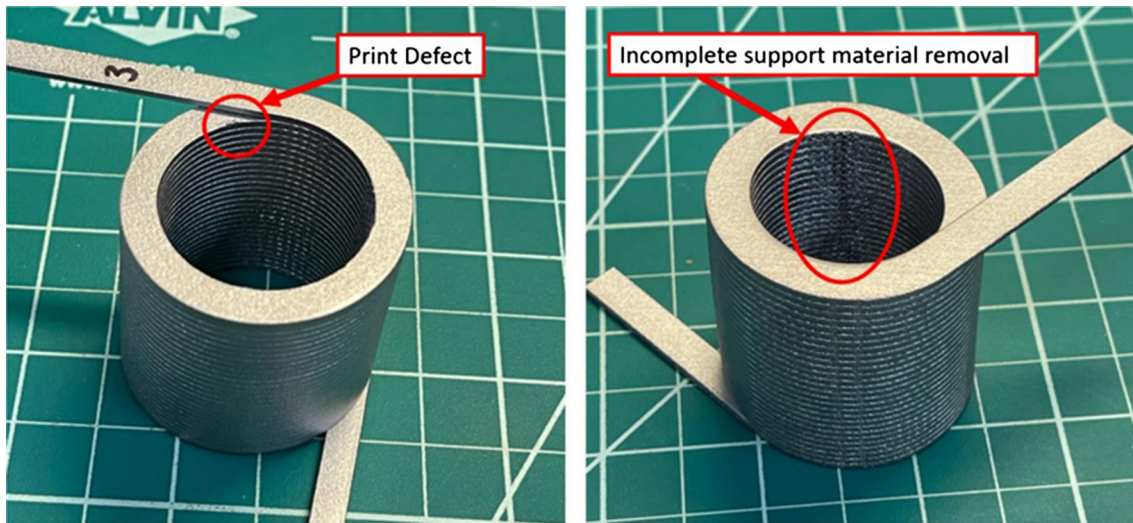


Fig. 5 Defects upon inspection of a spring from AM Vendor 1

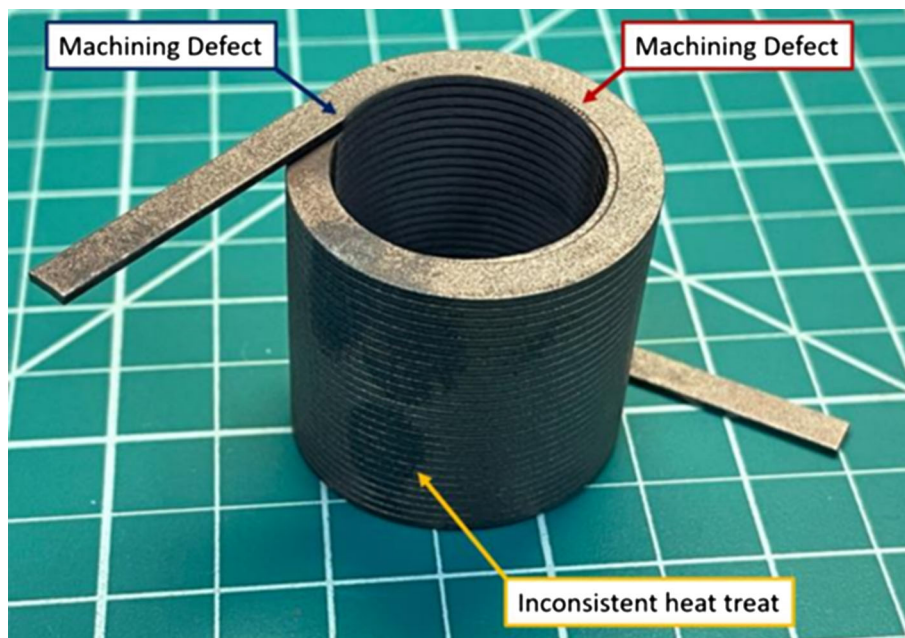


Fig. 6 Defects upon inspection of a spring from AM Vendor 2

particle size distribution (PSD) between 15 and 45 μm . Layer size was 40 μm . After printing, the springs were heat treated at 490 $^{\circ}\text{C}$ for 6 h in air. Specific print details from Vendor #2 were kept proprietary. However, it is expected that standard EOS parameters were used for EOS MS1 powder.

Inspection of the as-printed hardware displays various print defects. Interestingly, print defect types differ between vendors. Vendor #1's springs primarily display defects generated by the printing process itself. Figure 5 displays these defects. Vendor #2's defects appear to have been generated by the post-processing of the hardware and are shown in Fig. 6.

Dimensional inspection allows for insights into the repeatability of printing this material as well as the geometric tolerances of the as-printed parts. Of all the dimensions printed, the vast majority of dimensions met tolerance requirements, matching those of the traditionally fabricated spring. Further-

more, when comparing the masses of the traditionally fabricated springs to that of the AM springs with similar geometries, the masses were proportional to differences in material density. The AM spring on average weighed 0.184 kg (EOS MS1 material density of 8000 kg/m^3) and the traditional spring weighed 0.181 kg (17-7 steel material density of 7806 kg/m^3). Figure 7 summarizes inspection findings of major spring dimensions.

6.2 Experimental Test Setup

To test the spring torque performance, a bench-top test setup was built utilizing a hand-held calibrated torque dial and custom tooling mounted to an optical bench. This test setup allowed the axis of rotation to remain unconstrained, but allowed the upper spring arm to be driven with a measured

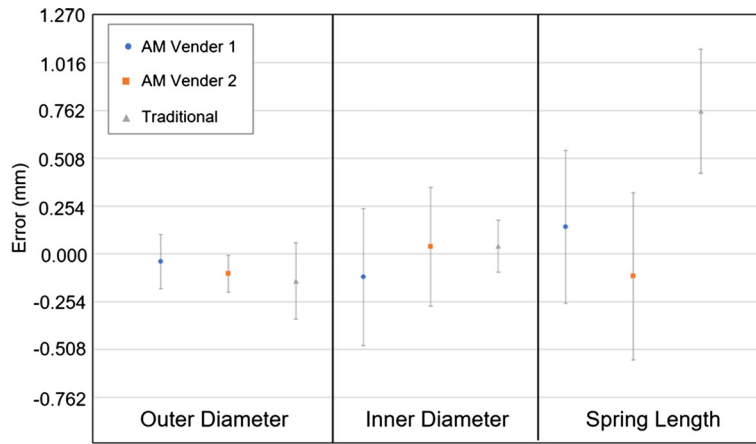


Fig. 7 Inspection of spring major dimensions. This inspection demonstrated that all AM parts as fabricated achieve required geometric tolerances for major dimensions.

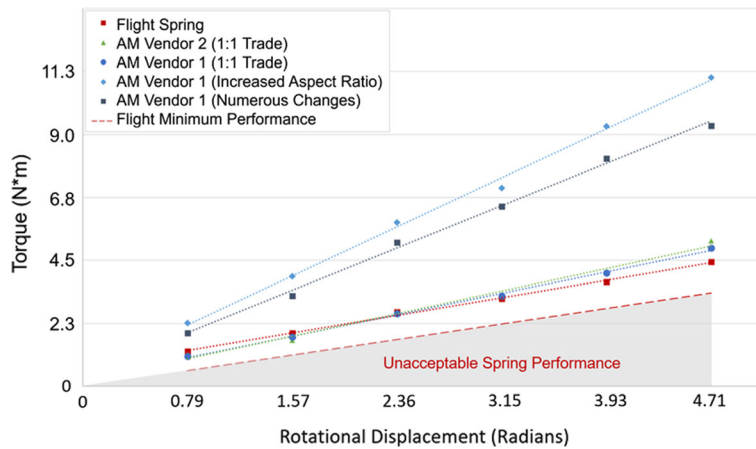


Fig. 8 Average spring torque output with respect to displacement



Fig. 9 Tensile coupons shown as printed and after machining

torque value. The torque dial used had an uncertainty of 0.28 N*m.

6.3 Torque and Life-Cycle Testing Results

A series of springs were manufactured that incrementally differed from the traditionally fabricated spring. This will allow each design change to be studied incrementally. Sixteen

additively manufactured springs were tested and compared to six traditionally manufactured springs in the same bench-top test setup. This allowed performance to be compared directly. Table 3 summarizes the test results. Figure 8 provides a visual representation of torque output with respect to displacement. For all springs, experimental performance slightly exceeded design performance. The springs with increased radial height

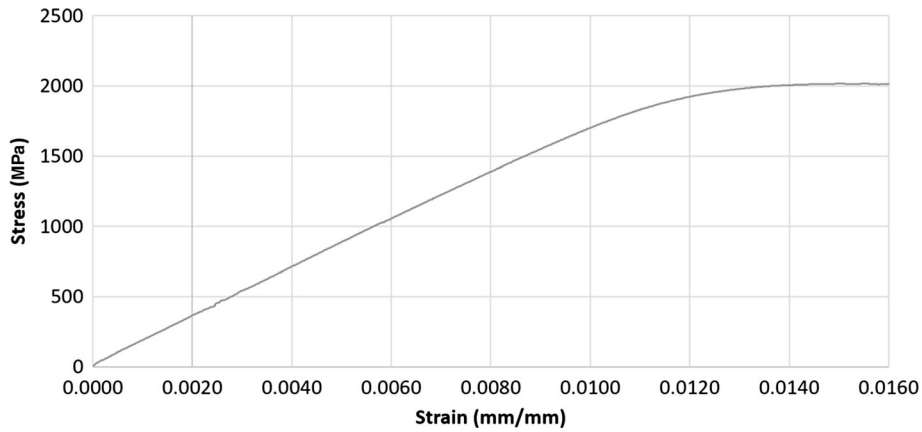


Fig. 10 Average stress–strain test results for tensile coupons

Table 4 Tensile test result summary

	Units	As-printed AM maraging steel	Expected AM MS1
Elastic modulus	GPa	176.5	180.0
Yield strength	MPa	1999	1986
Ultimate strength	MPa	2020	2048
Source		<i>As-tested</i>	<i>Matweb (Ref 10)</i>

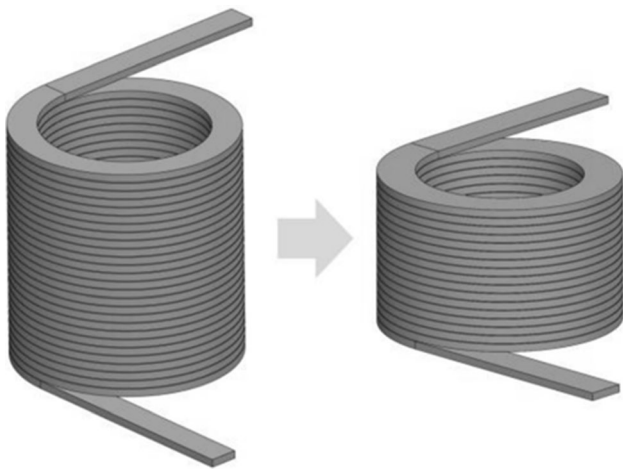


Fig. 11 Flight spring design compared to zero stress margin AM spring design

showed a 148% increase in torque output at 4.71 radians of displacement and a 117% increase spring constant compared to the flight springs. Four units of each spring design were tested and with a standard deviation of 0.43 N*m or less for each design. Higher standard deviations were generally associated with higher displacement.

Additionally, life-cycle testing was conducted on two of the springs. Life-cycle testing is defined as functional testing through at least three times the number of expected cycles needed in application. For the SWOT and NISAR missions, roughly 20 cycles of the spring mechanism are needed for ground testing and flight applications. Therefore, a life-cycle test must apply at least 60 cycles on the springs. Two springs were tested through 80 cycles of winding and unwinding, no degradation in torque was witnessed.

6.4 Material Testing

During printing at AM Vendor #1, twelve tensile coupons were printed from two lots of springs. These tensile coupons were then machined down and tensile tested to failure per ASTM E8 “Standard Test Methods for Tension Testing of Metallic Materials.” Figure 9 shows the tensile coupons before and after machining. Figure 10 displays stress–strain curves. Testing results were slightly lower than expected material properties. Table 4 summarizes the testing results. A larger data set would be needed to create reliable material allowables.

7. Conclusion and Future Implications

This report has successfully demonstrated AM torsion springs at the component level in a laboratory environment. The major conclusion points are:

- Additive manufacturing enables novel torsion spring geometries to be fabricated.
- Testing confirms that AM springs match expected design performance.
- Existing AM materials are comparable to high-performance spring materials but require additional considerations (e.g., material allowable testing and post-processing).

Based on this work, it is possible to extend the research. First, it is possible to minimize mass and volume by redesigning the springs. Second, it is possible to minimize part count. Testing has demonstrated that for the AM springs a 1.2×7.0 mm cross section allows for increased torque performance while maintaining necessary stress margins. With this information, it is possible to hold the spring cross section constant, and modify the number of coils to minimize mass and volume while

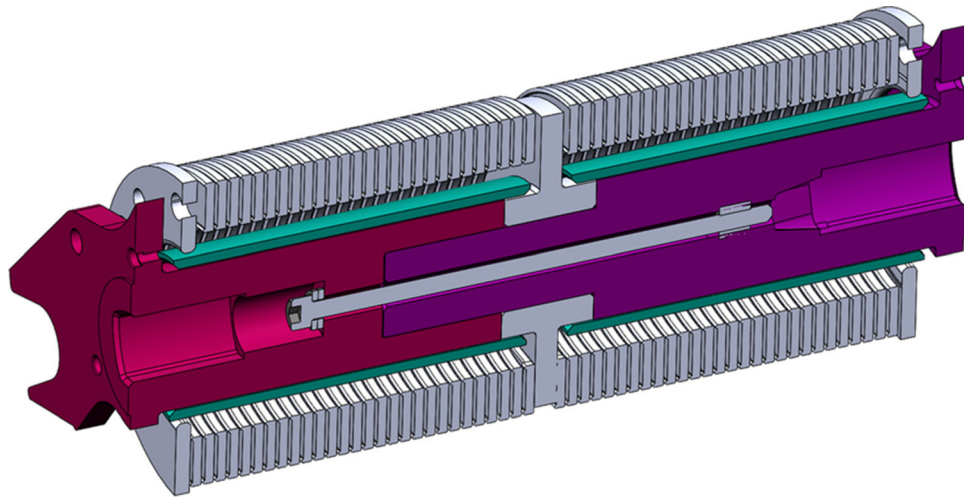


Fig.12 Structurally embedded spring with nine total parts demonstrates reduction in part count when compared to traditional manufacturing methods

maintaining acceptable stress margins. As such, it is possible to manufacture a spring that has 17.25 body coils (seen in Fig. 11), and maintains positive stress margin with the following performance:

- o Decrease mass by 23% compared to flight hardware
- o Decrease spring axial length by 52% compared to flight hardware
- o Increase spring rate by 167% compared to flight hardware.

Part count can be minimized by embedding the spring in the surrounding structure. Using AM manufacturing, it is possible to minimize the part count from 24 parts to 9 parts in the spring mechanism. This is partially achieved by printing both springs in the same piece part. Thus, a single part remains redundant with two individual complaint elements. Figure 12 demonstrates this part reduction when compared to Fig. 2. Part count reduction can reduce manufacturing, inspection, and testing costs. The steps below are needed to mature the technology for spaceflight.

- o A full environmental test campaign of the mechanism is needed to confirm findings in this report and achieve NASA Technology Readiness Level of 6. (Ref 12)
- o A standard, rigorous process for NDI of AM compliant elements needs to be developed. This will ensure that parts do not have unseen defects that could cause pre-mature failure. This is expected to be part of upcoming NASA AM design standards. (Ref 13, 14)

Post-processing manufacturing methods will need to be studied further for potential performance improvements. Decreasing as-printed surface roughness with chemical etching will likely increase hardware cycle life. Corrosion-resistant coatings would also protect maraging steel from stress fracture when exposed to corrosive environments.

References

1. T. Wholers, T. Gormet. History of Additive Manufacturing. (Wholers Report, 2015), <http://www.wholersassociates.com/history2014.pdf> [cited 8 December 2019]
2. Aerojet Rocketdyne's Family of 3d-Printed Rocket Engines, (Aerojet Rocketdyne, 2019), <https://www.rocket.com/innovation/bantam> [cited 8 December 2019]
3. Case Study PIXL Mars Rover. (Carpenter Additive, 2020), https://f.hubspotusercontent10.net/hubfs/6205315/Resources/Case%20Study/20210122-CT-Mars-Rover-Case-Study_F.pdf?hsCtaTracking=aa07829b-5b60-474e-92de-36d99da655f7%7C41643ab9-681e-4065-9066-4362fc3a85dd [cited 12 April 2021]
4. Overview. (National Aeronautics and Space Administration, 2020), <https://swot.jpl.nasa.gov/mission/overview/> [cited 12 April 2021]
5. Mission Concept. (National Aeronautics and Space Administration, 2020), <https://nisar.jpl.nasa.gov/mission/mission-concept/> [cited 12 April 2021]
6. P. Lytal, M. Renson. Spacecraft Common Deployable Boom Hinge Deploy and Latching Mechanisms, in *Proceedings of the 44th Aerospace Mechanism Symposium*, pp 403–416 2017
7. C.Gebara, and P. Lytal. Multi-Mission Deployable Boom: Spring Mechanism Failure Investigation and Solution, in *Proceedings of the 45th Aerospace Mechanism Symposium*, 2020
8. R.G. Budynas and J.K. Nisbett, *Shigley's Mechanical Engineering Design*, 9th ed. McGraw-Hill, New York, 2008
9. A.M. Wahl, *Mechanical Springs*, 1st ed. Penton Publication Company Cleveland, Ohio, 1944
10. EOS MS1 Maraging Steel Sintered on EOSINT M 270. (MatWeb Material Property Data. Matweb LLC) <http://www.matweb.com/search/DataSheet.aspx?MatGUID=e9f7cb19eb81450d8f67966151bd1802&cck=1#:~:text=EOS%20Maraging%20Steel%20MS1%20is,obtain%20excellent%20hardness%20and%20strength>
11. T. Debroy, et al. Additive manufacturing of metallic components—Process, structure and properties, (*Progress in Materials Science*), <https://www.sciencedirect.com/science/article/pii/S0079642517301172#! Vol 92, March 2018> [cited 12 April 2021]
12. Technology Readiness Level, (National Aeronautics and Space Administration, 2020), https://www.nasa.gov/directorates/heo/scan/engineering/technology/technology_readiness_level [cited 12 April 2021]
13. E.Lanigan. A NASA Perspective on the Growing Role of In-Situ Process Monitoring in Managing Risk of AM Hardware, (NASA Marshall Space Flight Center, 2019), <https://ntrs.nasa.gov/api/citations/20200000032/downloads/20200000032.pdf> [cited 12 April 2021]

14. Additive Manufacturing Requirements for Spaceflight Systems, (National Aeronautics and Space Administration, 2021), <https://standards.nasa.gov/standard/nasa/nasa-std-6030> [cited 3 Dec 2021]

Publisher's Note Springer Nature remains neutral with regard to jurisdictional claims in published maps and institutional affiliations.